RSC Advances

ROYAL SOCIETY OF CHEMISTRY

www.rsc.org/advances

Preparation and characterization of magnetic nanocomposite catalysts with double Au nanoparticle layers

Zia Ur Rahman[a], Tingting Zhang[a,b], Siwen Cui[a,b], Daoai Wang*[a]

[a]*State Key Laboratory of Solid Lubrication, Lanzhou Institute of Chemical Physics, Chinese Academy of Sciences, Lanzhou 730000, China*

[b]*University of the Chinese Academy of Sciences, Beijing 100049, China*

Abstract

In this paper magnetic nanocomposite catalysts, with single gold catalytic layer (Fe_3O_4@SiO_2-Au and Fe_3O_4@SiO_2-Au@mSiO_2), double gold catalytic layers (Fe_3O_4@SiO_2-Au@mSiO_2-Au), and with one gold layer and one silver layer (Fe_3O_4@SiO_2-Au@mSiO_2-Ag), were prepared through simple steps. Different techniques were used for characterization of the as prepared nanocomposite catalysts, such as transmission electron microscopy (TEM), X-ray diffraction (XRD), vibrating sample magnetometer (VSM), energy-dispersive X-ray spectroscopy (EDX) *etc*. Catalysts were used for the catalytic reduction of 4-nitrophenol (4-NP) to 4-aminophenol (4-AP) in the presence of $NaHB_4$. All nanocomposite catalysts showed very good catalytic activity; however the nanocomposites with double catalytic layers (Fe_3O_4@SiO_2-Au@mSiO_2-Au and Fe_3O_4@SiO_2-Au@mSiO_2-Ag) showed excellent catalytic activity for the reduction reaction of 4-nitrophenol. Due to the magnetic core, nanocomposite catalysts showed magnetic properties and can be easily separated and recycled for many times without any loss in activity. In case of nanocomposite catalysts with Au nanoparticles protected by silica (Fe_3O_4@SiO_2-Au@mSiO_2) indicated better recyclability as compared to other nanocomposites.

* Corresponding Author: E-mail: wangda@licp.cas.cn

1. Introduction

The development of catalysts with efficient stability and catalytic activity for potential applications in the field of catalysis has been an important aim of chemists and materials scientists due to economic reasons on one hand and environmental reasons on the other hand. For this purpose recently significant research has been carried out on transition metal nanoparticles, especially the noble metals, to improve their catalytic activity by controlling the size, shape, structure, and composition. Noble metals such as Au and Ag nanoparticles, due to their unique properties, have been utilized in the field of catalysis. To achieve better catalytic activity and recyclability these nanoparticles have been deposited on the surface of various supports like polymers,[1,2] carbon nanotubes,[3,4] graphene oxide,[5,6] hydrogels,[7,8] zeolites,[9,10] and metal oxides.[11-13] However, separation of these materials using traditional separation methods of filtration and centrifugation is difficult and time consuming. These methods are also not suitable for the separation of particles having sizes less than 100 nm,[14] thus hindering their recovery and recyclability.[15]

Iron oxide nanoparticles, due to the magnetic property, are therefore widely used as catalyst supports instead of conventional materials. These catalysts with magnetic property can be easily separated using an external magnet and are recycled.[16,17] The direct attachment of noble metals on iron oxide nanoparticles is difficult because of the different nature of the two materials. Some organic polymers, such as polyanniline, polypyrrole and poly (allylamine hydrochloride), have been used to attach Au nanoparticles on to iron oxide nanoparticles.[18-20] However, silica due to its large surface area, high and thermal stability, biocompatibility and good surface chemistry, has been widely used for the attachment of Au and Ag nanoparticles on the surface of Fe_3O_4 nanoparticles.[21-24] Silica not only prevents the aggregation of nanoparticles which is very important for nanocomposite catalysts in their better activity, but also provides silanol groups for further modification. However due to –Si-OH groups on the surface of silica, it is negatively charged which is not suitable for the adsorption of Au nanoparticles. It is functionalized with some groups, such as amine groups, which can readily adsorb Au nanoparticles.

Nitrophenols and their derivatives are organic pollutants which result from production of synthetic dyes, pesticides, insecticides and herbicides.[25] These compounds occur in industrial and agricultural waste

waters and cause significant pollution. While 4-NP is a reducing agent and has many applications in photography, dyes, medicines, corrosion inhibition *etc*.[26] Thus the reduction of nitrophenols to aminophenols is of utmost importance due to many applications of aminophenols in various industries on one hand and controlling the pollution caused by nitrophenols on the other hand. Noble metals such as Au, Ag, Pt, Pd *etc*. have been used as catalysts for the reduction reaction of nitrophenols to aminophenols.[27-31]

Different approaches were employed not only to stabilize the catalysts for using under harsh reaction conditions but also reusing for many cycles without reduction in their catalytic activity which are very important for catalysts. Recently a core-shell strategy was employed to make gold nanocomposite catalyst stable. It was found that the uniform shell of gold on silica coated iron oxide nanoparticles not only made its catalytic activity better but also its stability and recyclability.[32] Stabilization of gold catalysts was achieved using yolk/shell structure also known as nanorattles by Lee *et al*. In this case Au nanoparticles were used as cores and silica as shell.[33] Similarly; Ge *et al.* used core-satellite structure, using silica shell to protect the catalyst. Silica was etched using NaOH solution to produce pores in it.[34] Nanocomposite catalysts with magnetic iron oxide as core and mesoporous silica shell with gold nanoparticles inside silica have also been reported. Mesoporous silica was achieved using organic templates to produce mesopores which allowed reactants to pass through and react on the surface of Au nanoparticles.[27,35]

But the reported methods either involve complex procedures or while improving the stability of the catalysts the activity is affected. It, therefore, still remains a challenge not only to improve the stability of the catalyst but also its catalytic activity as well as recyclability. Here we report simple steps to prepare magnetic nanocomposite catalysts with single and double catalytic layers. The nanocomposites catalysts have good catalytic activity and recyclability.

2. Experimental

2.1. Materials

Ferric chloride hexahydrate ($FeCl_3 \cdot 6H_2O$) and Sodium borohydride ($NaBH_4$) were obtained from Kermal, Tianjin Chemical Reagent Co., Ltd. Tetraethyl orthosilicate (TEOS) was purchased from Sigma-Aldrich. Tetrachloroauric acid tetrahydrate ($HAuCl_4 \cdot 4H_2O$) was obtained from Chengdou Chemical

Reagent Co., Ltd. Trisodium citrate dihydrate ($C_6H_5Na_3O_7 \cdot 2H_2O$) was provided by Xilong Chemical Company, China. 3-Aminopropyl-triethoxysilane (APTES) was purchased from Aladin, Shanghai (China). Sodium acetate anhydrous (CH_3COONa), Cetyltrimethylammonium bromide (CTAB), Silver nitrate ($AgNO_3$), and 4-Nitrophenol (4-NP) were obtained from Sinopharm Chemical Reagent Co., Ltd. (Shanghai, China). All other chemicals were of analytical grade and used as received. Deionized water was used throughout the experiment.

2.2. Methods

2.2.1. Synthesis of magnetic Fe_3O_4 nanoparticles

Solvothermal method was used to prepare Fe_3O_4 nanoparticles by mixing 2.02 g of $FeCl_3 \cdot 6H_2O$ and 4.10 g of sodium acetate in 50 mL of ethylene glycol and stirring for 30 min. Yellow mixture obtained was then heated in a Teflon-lined stainless-steel autoclave at a temperature of 200 °C for 10 h. After cooling the autoclave naturally to room temperature the black nanoparticles were separated and washed with distilled water and ethanol for three times each, then dried in vacuum at 60 °C.

2.2.2. Synthesis of Fe_3O_4@SiO_2 and APTES-modified Fe_3O_4@SiO_2 nanocomposites

A thin shell of silica was coated on the surface of iron oxide nanoparticles using sol-gel method by dispersing 0.10 g of Fe_3O_4 nanoparticles in a mixture of ethanol (80 mL) and water (20 mL) through ultrasonication for few minutes. To this mixture ammonia solution (3.0 mL, 28 wt %) was added followed by the addition of 80 μL TEOS very slowly and was kept stirring at room temperature for 10 h. The above particles (0.13 g) were refluxed for 10 h with APTES (1.50 mL) in toluene for functionalization with amine groups.

2.2.3. Synthesis of Au nanoparticles

Citrate-stabilized Au nanoparticles were prepared as reported before.[36] Briefly, 100 mL of $HAuCl_4$ (5.0×10^{-4} M) aqueous solution was heated while stirring and 5 mL (1 wt %) trisodium citrate was added when it started boiling. The color of solution changed from pale yellow to violet and then to deep red indicating the formation of Au nanoparticles. The mixture was stirred for further 30 min and then cooled

to room temperature under stirring. The red wine color Au nanoparticles have absorbance maximum at 520 nm with size of about 15 nm.

2.2.4. Preparation of Fe_3O_4@SiO_2-Au and Fe_3O_4@SiO_2-Au@mSiO_2-Au

In order to prepare Fe_3O_4@SiO_2-Au nanocomposites, a dispersion (50 mL) of amine-functionalized Fe_3O_4@SiO_2 (0.04 g) was mixed with 100 mL of Au nanoparticles through ultrasonication and stirred for 4 h at ambient temperature. To prepare Fe_3O_4@SiO_2-Au@mSiO_2-Au, with double catalytic layers, another layer of mesoporous silica was coated on the surface of Fe_3O_4@SiO_2-Au by dispersing these nanocomposites (0.05 g) in ethanol (60 mL) and water (80 mL) mixture with 0.30 g of CTAB and 2 mL of ammonia solution. The mixture was mechanically stirred at 30 °C for 30 min then TEOS (0.8mL) in ethanol was added dropwise and continued stirring for 8 h. CTAB was removed by refluxing these nanocomposites in acetone for 48 h for three times.[37] The prepared nanocomposites were then reacted with APTES in isopropanol at 80 °C for 2 h. These nanocomposites with amine groups on the surface were reacted with Au nanoparticles to prepare nanocomposites with double Au nanoparticle layers, Fe_3O_4@SiO_2-Au@mSiO_2-Au, as before. Similarly, Fe_3O_4@SiO_2-Au@mSiO_2-Ag, nanocomposites with silver nanoparticles as co-catalysts were prepared by reacting Fe_3O_4@SiO_2-Au@mSiO_2 (0.025g) with 100 mL of silvering mixture containing $AgNO_3$ (4 mM) in ethanol and n-butylamine (4 mM) in equal ratio at 50 °C for 2 h in a polypropylene flask. At each step of preparation the nanocomposites were washed with water and ethanol and then dried in vacuum at 60 °C.

2.2.5. Catalytic reduction of 4-Nitrophenol (4-NP)

The reduction reaction of 4-NP with $NaBH_4$ was used as a model reaction to investigate the catalytic behavior of the prepared nanocomposites. Typically equal amount of 4-NP (0.2 mM) and freshly prepared $NaBH_4$ (80 mM) were mixed and then a very small amount of the prepared nanocomposites (3.33×10^{-5} gmL^{-1}) added to this mixture. The progress of reduction reaction was monitored by measuring the absorption spectra at certain interval of time. The reactions and their absorption measurements were done at room temperature for all nanocomposites.

2.2.6. Characterization

The morphology of the nanoparticles and nanocomposites was determined by FEI Tecnai G2 TF20 transmission electron microscope (TEM) with field emission gun operated at 200 kV and Hitachi S-4800 scanning electron microscope (SEM) (Japan). Magnetic properties of the samples were measured at room temperature using vibrating sample magnetometer (VSM, Lakeshore 730). X-ray diffraction (XRD) analysis was carried on an X'Pert pro Philips X-ray diffractometer with Cu Kα radiation (λ = 1.5406 Å) and scan range (2θ) was from 10^{o} to 90^{o}. FT-IR measurements were carried out at room temperature on a Nicolet Nexus 670 FT-IR spectrometer (GMI Inc., MN, America). Zeta potential was carried out using a Zetasizer Nano ZS/ZEN 8600 (Malvern instruments). X-ray photoelectron spectra (XPS) were done on Thermo Scientific ESCALAB 250xi with a monochromatic Al Kα X-ray source operated at 200 W. The Brunauer-Emmett-Teller (BET) surface area and pore size distribution were measured with Autosorb-iQ analyzer (Quantachrome Instruments, U.S.) at 77 K. Sample was treated under nitrogen at 453 K for 5 h before measurements. Pore size distributions were calculated by the Barrett-Joyner-Halenda (BJH) method. The gold and silver content of the samples was determined using the inductively coupled plasma (ICP) on a Varian AA240 analyzer. A double beam spectrometer, UV-2600, Shimadzu (Japan) was used to measure the absorption spectra.

3. Results and discussion

3.1. Characterization of the nanocomposites

Different techniques were employed to characterize nanoparticles and nanocomposites. The morphology of iron oxide nanoparticles prepared through solvothermal method is shown in Fig. 1. From TEM and SEM results the particles can be seen as spherical in shape having a wide range of size (200-400 nm). The outer rough surface indicates that these particles are formed of many nanocrystals. TEOS, a silica precursor, was used to coat the surface of iron oxide nanoparticles with a thin shell (~30 nm) of silica through sol-gel process. By reacting with APTES the surface of silica coated iron oxide nanoparticles became functionalized with amine groups. Amine functional groups on the surface of silica coated iron oxide nanoparticles are important for the attachment of negatively charged gold nanoparticles. FT-IR spectra of iron oxide nanoparticles, nanoparticles after silica coating, and amine functionalized

silica coated iron oxide nanoparticles are shown in Fig. S1 (Supplementary Information). The peaks appearing at 582 and 3421 cm^{-1} in the spectra of Fe_3O_4 nanoparticles are due to the Fe-O, and hydroxyl groups respectively. The new absorption peaks after silica coating were Si-O-Si (1076 cm^{-1}), Si-O (443 cm^{-1}), and the surface silanol groups Si-OH (955 cm^{-1}) (Fig. S1b). After reaction with APTES the bands arising from Si-O groups are at 1154 and 1080 cm^{-1} which can be clearly seen. The bands appearing at 2850 cm^{-1} and 2925 cm^{-1} are assigned to C-H stretching vibration of the methylene group. The broad band appearing at 3431 cm^{-1} is due to the N-H stretching vibration, while the other at 1631cm^{-1} is due to the N-H bending mode of amino group (Fig. S1c). XPS, an important technique to give information about the surface elements, was also carried out for silica coated nanoparticles after reaction with APTES to complement the results of FT-IR (Fig. 2). An obvious and clear peak at 399.4 eV appeared which is due to N 1s (Inset of Fig.) also confirmed the successful reaction of APTES with silica surface resulting in attachment of amine groups, while other peaks such as C 1s, O 1s, Fe 2p and Si 2p were also shown. In order to further confirm the attachment of amine groups and surface charge of amine functionalized silica coated iron oxide nanoparticles, zeta potential analysis was carried out. Zeta potential measurement was important because amine groups were introduced on silica surface, while silica is negatively charged due to silanol groups and does not favor the adsorption of citrate stabilized negatively charged Au nanoparticles. The gold nanoparticles are mainly attached to alkylamines through electrostatic attraction.[33] From the results of zeta potential, measured at different pH, we can see that amine functionalized nanoparticles have high positive potential value (+21 mV) even at pH of 8 (Fig. S2). It therefore not only confirmed that amine groups are present on the surface of silica coated iron oxide nanoparticles but also showed that these particles are highly positively charged and the interaction between gold nanoparticles and the former is mainly electrostatic. Thus the prepared nanoparticles provide a suitable surface for the attachment of gold nanoparticles. Fig. 3 indicates the TEM images of nanocomposites with Au and Ag nanoparticles. From Fig. 3a, it is clear that the surface of Fe_3O_4@SiO_2 is almost completely covered with a large number of Au nanoparticles which can also be seen from inset of the figure showing a single particle. After coating another silica shell on these particles, Au nanoparticles can be seen inside a thick

shell of silica (~100 nm) after CTAB extraction (Fig. 3b). CTAB was used as porogen which was extracted by refluxing the nanocomposites with acetone, thus resulted in the formation of mesopores in silica shell. CTAB extraction was confirmed from the results of FT-IR spectra as shown in Fig. S3, which indicates that the bands at 2850 cm^{-1} and 2920 cm^{-1} were almost completely disappeared. It proved that most of the CTAB was extracted from silica shell. Mesoporous structure is very important because the mesopores allow reactants to pass and react on the surface of metal catalyst. The N_2 adsorption-desorption isotherms and pore-size distribution of mesoporous nanocomposites are shown in Fig. S4 (Supplementary Information). The BET surface area and pore volume measured are 138 m^2/g and 0.25 cm^3/g respectively. The type IV isotherm curve indicates that the nanocomposites with mesoporous silica shell possess a well defined mesoporous structure having a narrow pore size distribution with a mean size of about 2 nm as shown in the inset of figure. The nanocomposites with a second layer of Au nanoparticles or Ag on the outer silica shell are shown in Fig. 3c and Fig. 3d, respectively. From these results it was proved that the nanocomposites with single and double catalytic layers were successfully prepared, which is very clear from Fig S5 (Supplementary Information). Also high resolution transmission electron microscopy (HRTEM) images of these nanocomposites indicated that the size of Au nanoparticles is about 15 nm and that of Ag nanoparticles is about 12 nm with clear lattice fringes (Fig. S6, Supplementary Information).

The wide angle XRD patterns of iron oxide nanoparticles and gold caoted iron oxide nanocomposites are given in Fig. 4. The major peaks at 30.3°, 35.5°, 43.2°, 53.6°, 57.2°, and 62.7° were observed which are due to the diffraction from (220), (311), (400), (422), (511), and (440) planes of the face-centered cubic (fcc) lattice of Fe_3O_4 (JCPDS card no. 79-0418), respectively (Fig. 4a). These values confirm that the prepared iron oxide nanoparticles are pure with good crystallinity. The peaks at 38.2°, 44.4°, 64.5°, and 77.7°, corresponding to (111), (200), (220), and (311) lattice planes respectively, of the cubic-phase gold, indicating the attachment of gold nanoparticles to silica coated iron oxide nanoparticles. All the three samples with gold nanoparticles show the characteristic peaks of Au (Fig. 4b-d). Similarly XRD analysis revealed the characteristic peaks of Ag in Fe_3O_4@SiO_2-Au@mSiO_2-Ag which can be clearly seen in Fig. S7 (Supplementary Information). It confirmed the attachment of silver nanoparticles

on the surface of Fe_3O_4@SiO_2-Au@mSiO_2, with inner Au nanoparticles layer. The formation of the hybrid nanocomposites with both Au and Ag was further verified by high-angle annular dark-field scanning transmission electron microscopy (HAADF-STEM) imaging and elemental mapping as shown in Fig. 5. Energy-dispersive X-ray spectroscopy (EDX) technique was also used to know about the elements present in the nanocomposites (Fig. S8, Supplementary Information). The precursor elements in nanocomposites such as Fe, Si, O, Au, and Ag can be seen from the spectra. The amount of Au and Ag in the nanocomposites was measured through ICP and is given in the Table S1 (Supplementary Information).

3.2. Catalytic activity of the nanocomposites

The catalytic activity of nanocomposites was investigated for the catalytic reduction of 4-nitrophenol (4-NP) in the presence of $NaBH_4$, a basic reaction used to monitor the catalytic activity of metal nanoparticles as catalysts.[25,38,39] The kinetics of the reaction can be monitored by measuring the absorption spectra at specific interval of time using UV–vis spectroscopy. The light yellow solution of 4-NP alone has a peak at 317 nm, however after the addition of $NaBH_4$ the mixture shows a red shifted peak at 400 nm, which is the characteristic absorption peak of 4-nitrophenolate ions in alkaline solution as shown in Fig. 6 .[40,41] The absorbance of the mixture remained the same without any change indicating no reduction occurred even for many hours without the addition of any nanocomposite. It confirmed that the reaction does not proceed by $NaHB_4$. Similarly no reduction reaction took place in the presence of iron oxide nanoparticles or silica coated iron oxide nanoparticles. However after the addition of small quantity of the nanocomposites catalysts with Au nanoparticles or Ag nanoparticles, the reduction reaction took place and completed very quickly. UV-vis spectra of mixture in the presence of nanocomposites catalysts are shown in Fig. 7, from which we can see that the absorption peak at 400 nm decreases and another peak at 300 nm appears. This new peak is due to the formation of 4-aminophenol (4-AP) as a result of this reaction. Due to the complete reduction reaction the mixture becomes colorless and the peak at 400 nm completely disappears. An isosbestic point shown by the UV-vis spectra between the two absorption bands indicates that only one product (4-AP) is produced during the reduction of 4-NP.[26] As from Fig. 7a,

we can see that in the presence of Fe_3O_4@SiO_2-Au the reaction goes to completion (~98 % conversion) in 16 minutes. Similarly, in case of Fe_3O_4@SiO_2-Au@mSiO_2 the reaction is slow and took 30 minutes for reduction of 4-NP. This is due to the silica shell which slows down the diffusion of reactants.[27] However, in case of Fe_3O_4@SiO_2-Au@mSiO_2-Au and Fe_3O_4@SiO_2-Au@mSiO_2-Ag, due to double catalytic layers, the reaction goes to completion just within 7 and 4 minutes respectively. Since the concentration of $NaBH_4$ is very high as compared to 4-NP (C($NaBH_4$)/C(4-NP) = 400:1), therefore its concentration remains constant throughout the reaction. The rate of reaction thus follows pseudo first-order kinetics and depends only on the concentration of 4-NP. The rate constant (k) for each nanopcomposite can be measured from the slope of the straight line resulting from relationship between ln (C_t/C_0) *versus* time, Fig (8a-d). Where C_t and C_0 are the concentration values of 4-NP at time t and 0 respectively, which are obtained from the respective absorbance values at time t and 0, (A_t/A_0). The straight lines proved that the reaction follows first-order kinetics. The rate constants (k) of nanocomposites calculated from their corresponding absorption spectra are 0.20, 0.10, 0.53 and 0.95 min^{-1} for Fe_3O_4@SiO_2-Au, Fe_3O_4@SiO_2-Au@mSiO_2, Fe_3O_4@SiO_2-Au@mSiO_2-Au, and Fe_3O_4@SiO_2-Au@mSiO_2-Ag respectively (Table S1, Supplementary Information). It indicated that both nanocomposites with double noble metal layers are better catalysts with higher rate constants as compared to others. Double catalytic layers are important because if the surface Au or Ag nanoparticles are detached after using for many cycles we still have another layer of Au nanoparticles which is protected by mesoporous silica and can be reused for further catalysis. The Turnover frequency (TOF) for all nanocomposites was also measured and is given in Table S1 (Supplementary Information). It can be seen that nanocomposites with both Au and Ag showed the highest TOF (81.52 h^{-1}). The difference in catalytic activity of Fe_3O_4@SiO_2-Au@mSiO_2-Au and Fe_3O_4@SiO_2-Au@mSiO_2-Ag might be due to the small difference in size of the noble metals, the latter having smaller Ag nanoparticles than the former with Au nanoparticles as indicated in HRTEM (Fig. S6, Supplementary Information). The catalytic activity increases with decrease in size of the metal particles.[33] Therefore the double nanoparticle layers not only improved the catalytic activity but also recyclability.

Catalytic activity of the nanocomposites having single and double gold nanoparticles layers in the reduction reaction of 4-nitrophenol to 4-aminophenol is schematically shown in Fig. 9.

3.3. Magnetic property, reusability, and stability of the Nanocomposites

Magnetic property of the catalyst is of utmost importance in catalysis because it makes the separation of catalysts very easy from the reaction mixture, which are then reused. Fig. 10 shows the room-temperature saturation magnetization (M_s) values. From the curves it is clear that naked Fe_3O_4 nanoparticles have very high saturation magnetization (M_s) of 72 $emug^{-1}$. After coating with a thin shell of silica the value decreased to 62 emu/g for $Fe_3O_4@SiO_2$, however this value further decreased to 50 $emug^{-1}$ after the attachment of gold nanoparticles, $Fe_3O_4@SiO_2$-Au (Fig. 10c). After coating with another thick silica shell the M_s further decreased (38 $emug^{-1}$) for $Fe_3O_4@SiO_2$-Au@$mSiO_2$. The nanocomposites with double catalytic gold layers ($Fe_3O_4@SiO_2$-Au@$mSiO_2$-Au) have the least value of 33 $emug^{-1}$. However, it is still large enough for these nanocomposites to be easily separated with an external magnet (inset of Fig. 10). This decreased value of M_s is due to the non magnetic double silica layers and double Au nanoaparticle layers.

For reusing the nanocomposite catalysts, these catalysts were separated from the solution using external magnet and washed with ethanol and water before using for another cycle. Since a very small amount of nanocomposites was used, therefore to make the separation of nanocomposites easy their ratio along with the reactants was increased five times. For each cycle freshly prepared $NaBH_4$ was used and for each nanocomposite a specific time was fixed to measure UV-vis spectra for all cycles. From Fig. 11 it can be seen that all nanocomposites show good reusability and conversion efficiency for 4-nitrophenol even using for many cycles. All nanocomposites showed a conversion of 98 % even reusing for 5 cycles, which started to decrease for some nanocomposites. From figure it is clear that even after reusing for 12 cycles, nanocomposites still have significant catalytic activity. It was found that $Fe_3O_4@SiO_2$-Au-$mSiO_2$ showed 94 % conversion efficiency after using for 12 cycles which is more as compared to others such as $Fe_3O_4@SiO_2$-Au (81 %)，$Fe_3O_4@SiO_2$-Au-$mSiO_2$-Au (85 %) or $Fe_3O_4@SiO_2$-Au-$mSiO_2$-Ag (76 %). In

case of Fe_3O_4@SiO_2-Au-mSiO_2 nanocomposites, the gold nanoparticles catalysts are protected by mesoporous silica that is the reason for showing good recyclability, although the rate constant (k) is lesser than other nanocomposites. In case of other nanocomposites with surface metal catalysts, the decrease in conversion efficiency is due to the detachment of surface Au or Ag nanoparticles as well as loss of particles during washing and dispersing through ultrasonication, when reused for many cycles.[34,42,43] It is therefore suggested that nanocomposites with surface metal catalyst are better to be used where rate of reaction is important; however stable nanocomposite with protected metal catalysts are considered where recyclability is important. In order to know about the structure stability of the nanocomposites, TEM and XRD of the nanocomposites were measured after using for 6 cycles. From TEM results we can see that in case of Fe_3O_4@SiO_2-Au some of the Au nanoparticles have detached from silica surface while also some aggregates of the Au nanoparticles can be seen on the surface (Fig. 12a). This is also one of the reasons for lowering the catalytic efficiency of nanocomposites. Similarly, in case of Fe_3O_4@SiO_2-Au-mSiO_2-Au and Fe_3O_4@SiO_2-Au-mSiO_2-Ag, the results indicate that some of the outer noble metal nanoparticles have detached while the inner Au nanoparticles layer inside mesoporous silica shell remains unaffected. In case of Fe_3O_4@SiO_2-Au-mSiO_2 the Au nanoparticles layer is protected by outer silica showing more efficiency for catalysis even after using for many cycles which is in agreement with the results shown in Fig. 11. The XRD results indicated the peaks of Fe_3O_4 as well as Au and Ag nanoparticles even after using these nanocomposites for many times as shown in Fig. S9 (Supplementary Information). Thus it can be concluded from the results of TEM and XRD that these nanocomposites show good stability and can be reused for many cycles.

4 Conclusions

In summary magnetic nanocomposite catalysts with double gold nanoparticle layers were prepared through simple steps. First magnetic iron oxide nanoparticles were prepared which were then silica coated and treated with APTES for gold nanoparticles attachment. Another mesoporous silica shell was prepared on the surface of these nanocomposites which was accompanied by another layer of gold nanoparticles or silver nanoparticles. All nanocomposite catalysts showed better catalytic activity for

reduction of 4-NP, however nanocomposite catalyst with double gold layers (Fe_3O_4@SiO_2-Au@mSiO_2-Au) showed catalytic activity having rate constant more than Fe_3O_4@SiO_2-Au and Fe_3O_4@SiO_2-Au@mSiO, having single layers. Similarly, nanocomposite catalyst with inner Au nanoparticles and outer Ag nanoparticles as co-catalysts (Fe_3O_4@SiO_2-Au@mSiO_2-Au) showed the best catalytic activity. Magnetic Fe_3O_4 nanoparticles endow nanocomposites with magnetic property and therefore can be re-used for many cycles after separation from mixture with a magnet without reduction in catalytic activity. Fe_3O_4@SiO_2-Au@mSiO_2 is considered for good recyclability due to protected Au nanoparticles, although its catalytic activity is poor as compared to other nanocomposites. This study will find significant applications in the field of catalysis.

Acknowledgements

The authors are grateful for the financial support from NSFC (21303227, 21573259) and the "Hundred Talents Program" of Chinese Academy of Sciences.

References

1. G. L. Li, L. Q. Xu, K. G. Neoh and E. T. Kang, *Macromolecules*, 2011, **44**, 2365-2370.
2. X. Zhang and Z. Su, *Adv. Mater.,* 2012, **24**, 4574-4577.
3. X. Hu, T. Wang, X. Qu and S. Dong, *J. Phys. Chem. B*, 2005, **110**, 853-857.
4. I. Park, K. Lee, D. Jung, H. Park and Y. Sung, *Electrochim. Acta*, 2007, **52**, 5599-5605.
5. X. Zhou, X. Huang, X. Qi, S. Wu, C. Xue, F. Y. C. Boey, Q. Yan, P. Chen and H. Zhang, *J. Phys. Chem. C*, 2009, **113**, 10842-10846.
6. J. Huang, L. Zhang, B. Chen, N. Ji, F. Chen, Y. Zhang and Z. Zhang, *Nanoscale*, 2010, **2**, 2733-2738.
7. J. Hain, M. Schrinner, Y. Lu and A. Pich, *Small*, 2008, **4**, 2016-2024.
8. X. Q. Wu, X. W. Wu, Q. Huang, J. S. Shen, and H. W. Zhang, *Appl. Surf. Sci.*, 2015, **331**, 210-218.

9. G. Li, D. Enache, J. Edwards, A. Carley, D. Knight and G. Hutchings, *Catal. Lett.*, 2006, **110**,7-13.
10. M. Severance and P. K. Dutta, *J. Phys. Chem. C*, 2014, **118**, 28580-28591.
11. Z. W. Seh, S. Liu, M. Low, S.-Y. Zhang, Z. Liu, A. Mlayah and M.-Y. Han, *Adv. Mater.*, 2012, **24**, 2310-2314.
12. L. Li, E. S. G. Choo, X. S. Tang, J. Ding and J. M. Xue, *Acta Mater.*, 2010, **58**, 3825-3831.
13. F. Chen, Q. Chen, S. Fang, Y. Sun, Z. Chen, G. Xie and Y. Du, *Dalton Trans.*, 2011, **40**, 10857-10864.
14. J. Ge, T. Huynh, Y. Hu and Y. D. Yin, *Nano Lett.*, 2008, **8**, 931-934.
15. F. H. Lin and R. A. Doong, *J. Phys. Chem. C*, 2011, **115**, 6591-6598.
16. S. Shylesh, V. Schunemann and W. R. Thiel, *Angew. Chem., Int. Ed.*, 2010, **49**, 3428-3459.
17. M. Zhu, C. Wang, D. Meng and G. Diao, *J. Mater. Chem. A*, 2013, **1**, 2118-2125.
18. S. Xuan, Y. Xiang -J. Wang, J. C. Yu and K. C.-F. Leung, *Langmuir*, 2009, **25**, 11835-11843.
19. H. Zhang, X. Zhong, J. J. Xu and H. Y. Chen, *Langmuir*, 2008, **24**, 13748-13752.
20. L. Y. Wang, J. W. Bai, Y. J. Li and Y. Huang, *Angew. Chem., Int. Ed.*, 2008, **47**, 2439-2442.
21. M. Abbas, S. R. Toratia and C. G. Kim, *Nanoscale*, 2015, **7**, 12192-12204.
22. X. Du, J. He, J. Zhu, L. Sun and S. An, *Appl. Surf. Sci.* 2012, **258**, 2717-2723.
23. Z. Xu, C. Li, X. Kang, D. Yang, P. Yang, Z. Hou, and J. Lin, *J. Phys. Chem. C*, 2010, **114**, 16343-16350.
24. H. Liu, C. Lin, Z. Ma, H. Yu, and S. Zhou, *Molecules* 2013, **18**, 14258-14267.
25. S. Panigrahi, S. Basu, S. Praharaj, S. Pande, S. Jana, A. Pal, S. K. Ghosh and T. Pal, *J. Phys. Chem. C*, 2007, **111**, 4596-4605.
26. M. J. Vaidya, S. M. Kulkarni and R. V. Chaudhari, *Org. Process Res. Dev.*, 2003, **7**, 202-208.
27. Y. Deng, Y. Cai, Z. Sun, J. Liu, C. Liu, J. Wei, W. Li, C. Liu, Y. Wang and D. Zhao, *J. Am. Chem. Soc.*, 2010, **132**, 8466-8847.
28. J. Ge, T. Huynh, Y. Hu and Y. D. Yin, *Nano Lett.*, 2008, **8**, 931-934.

29. B. Naik, S. Hazra, V. S. Prasad and N. N. Ghosh, *Catal. Commun.*, 2011, **12**, 1104-1108.

30. P. Liu and M. F. Zhao, *Appl. Surf. Sci.*, 2009, **255**, 3989-3993.

31. S. D. Oh, M. R. Kim, S. H. Choi, J. H. Chun, K. P. Lee, A. Gopalan, C. G. Hwang, K. S. Ho and O. J. Hoon, *J. Ind. Eng. Chem.*, 2008, **14**, 687-692.

32. Z. U. Rahman, Y. Ma, J. Hu, Y. Xu, W. Wang, and X. Chen, *RSC Adv*., 2014, **4**, 5012-5020.

33. J. Lee, J. C. Park and H. Song, *Adv. Mater.*, 2008, **20**, 1523-1528.

34. J. Ge, Q. Zhang, T. Zhang and Y. Yin, *Angew. Chem., Int. Ed.*, 2008, **47**, 8924-8928.

35. Z. U. Rahman, Y. Dong, L. Su, Y. Ma, H. Zhang and X. Chen, *Chem. Eng. J.*, 2013, **222**, 382-390.

36. G. Frens, *Nat. Phys. Sci*., 1973, **241**, 20-22.

37. S. L. Gai, P. P. Yang, C. X. Li, W. X. Wang, Y. L. Dai, N. Niu and J. Lin, *Adv. Funct. Mater*., 2010, **20**, 1166-1172.

38. Y. Lu, Y. Mei, M. Drechsler and M. Ballauff, *Angew. Chem. Int. Ed.*, 2006, **45**, 813-816.

39. J. Lee, J. C. Park and H. Song, *Adv. Mater.*, 2008, **20**, 1523-1528.

40. K. Hayakawa, T. Yoshimura and K. Esumi, *Langmuir*, 2003, **19**, 5517-5521.

41. S. Praharaj, S. Nath, S. K. Ghosh, S. Kundu and T. Pal, *Langmuir*, 2004, **20**, 9889-9892.

42. J. Zheng, Y. Dong, W. Wang, Y. Ma, J. Hu, X. Chen, and X. Chen, *Nanoscale*, 2013, **5**, 4894-4901.

43. K. S. Shin, J. -Y. Choi, C. S. Park, H.J. Jang and K. Kim, *Catal. Lett*. 2009, **133**, 1-7

Figure Captions

Fig. 1 TEM (a) and SEM (b) images of iron oxide nanoparticles.

Fig. 2 XPS spectrum of Fe_3O_4@SiO_2-NH_2.

Fig. 3 TEM images of (a) Fe_3O_4@SiO_2-Au, (b) Fe_3O_4@SiO_2-Au@mSiO_2, (c) Fe_3O_4@SiO_2-Au@mSiO_2-Au, and (d) Fe_3O_4@SiO_2-Au@mSiO_2-Ag.

Fig. 4 The wide angle XRD patterns of (a) Fe_3O_4, (b) Fe_3O_4@SiO_2-Au, (c) Fe_3O_4@SiO_2-Au@mSiO_2, and (d) Fe_3O_4@SiO_2-Au@mSiO_2-Au.

Fig. 5 HAADF-STEM image of (a) Fe_3O_4@SiO_2-Au@mSiO_2-Ag nanocomposite and elemental maps of (b) Fe, (c) Si, (d) O, (e) Au and (f) Ag on the same nanocomposite.

Fig. 6 UV-vis absorption spectra of 4-nitrophenol (4-NP) taken (a) before and (b) after the addition of $NaBH_4$.

Fig. 7 UV-vis absorption spectra of the reduction of 4-NP by $NaBH_4$ in the presence of (a) Fe_3O_4@SiO_2-Au, (b) Fe_3O_4@SiO_2-Au@mSiO_2, (c) Fe_3O_4@SiO_2-Au@mSiO_2-Au, and (d) Fe_3O_4@SiO_2-Au@mSiO_2-Ag.

Fig. 8 Plot of $\ln(C_t/C_0)$ versus time for all nanocomposites, (a) Fe_3O_4@SiO_2-Au, (b) Fe_3O_4@SiO_2-Au@mSiO_2, (c) Fe_3O_4@SiO_2-Au@mSiO_2-Au, and (d) Fe_3O_4@SiO_2-Au@mSiO_2-Ag.

Fig. 9 Schematic representation of the reduction of 4-nitrophenol to 4-aminophenol on nanocomposites with single and double Au nanoparticle layers.

Fig. 10 Room temperature magnetic hysteresis curves of (a) Fe_3O_4, (b) Fe_3O_4@SiO_2, (c) Fe_3O_4@SiO_2-Au, (d) Fe_3O_4@SiO_2-Au@mSiO_2, and (e) Fe_3O_4@SiO_2-Au@mSiO_2-Au. Inset shows magnetic separation of Fe_3O_4@SiO_2-Au@mSiO_2-Au.

Fig. 11 Reusability of (a) Fe_3O_4@SiO_2-Au, (b) Fe_3O_4@SiO_2-Au@mSiO_2, (c) Fe_3O_4@SiO_2-Au@mSiO_2-Au, and (d) Fe_3O_4@SiO_2-Au@mSiO_2-Ag as catalysts for the reduction of 4-NP with $NaBH_4$.

Fig. 12 TEM images of (a) Fe_3O_4@SiO_2-Au, (b) Fe_3O_4@SiO_2-Au@mSiO_2, (c) Fe_3O_4@SiO_2-Au@mSiO_2-Au, and (d) Fe_3O_4@SiO_2-Au@mSiO_2-Ag after reusing for 6 cycles.

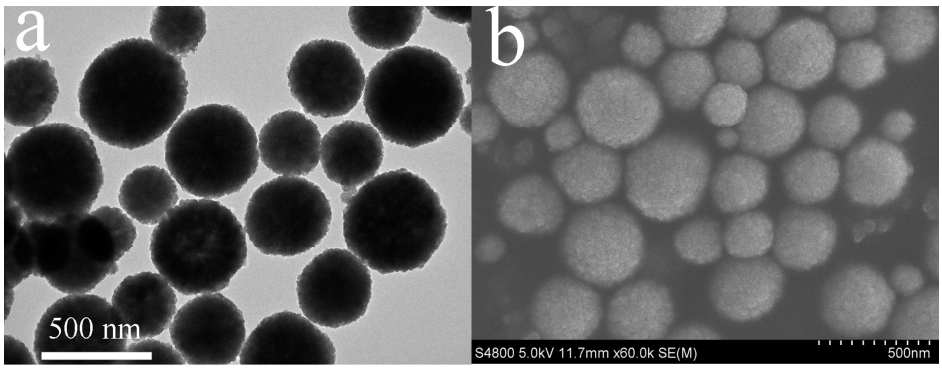

Fig. 1

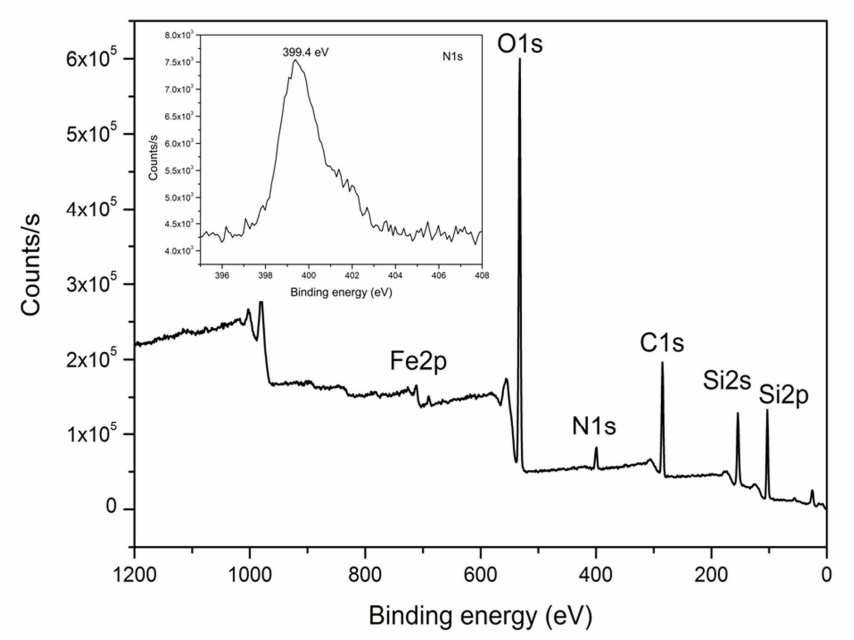

Fig. 2

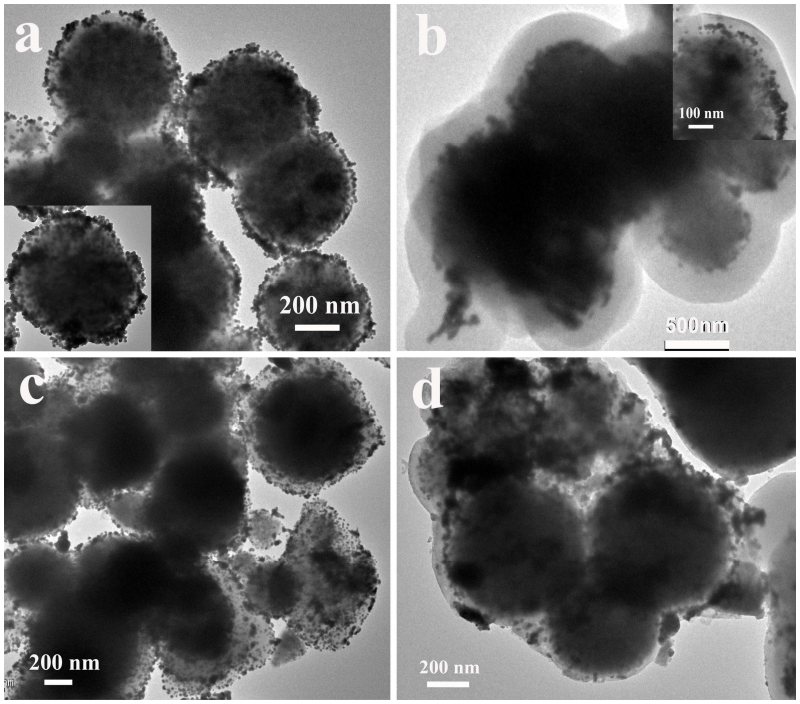

Fig. 3

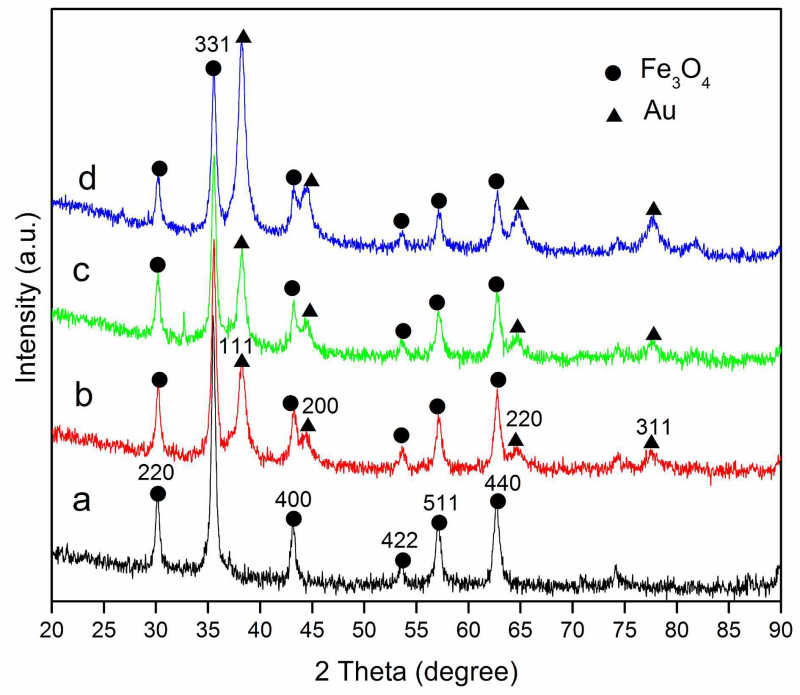

Fig. 4

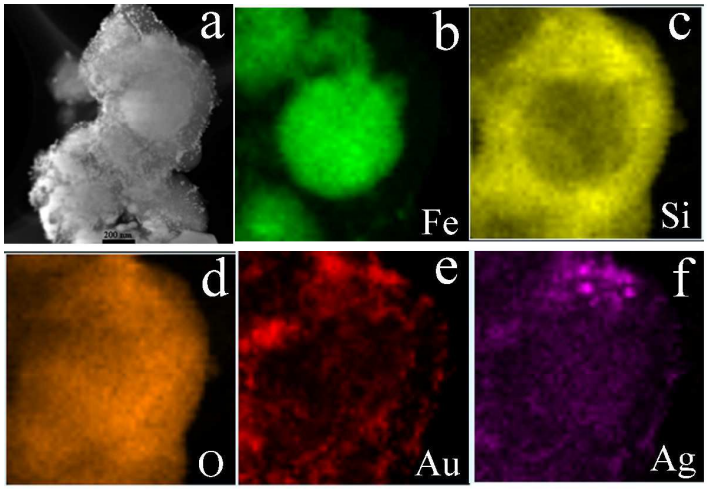

Fig. 5

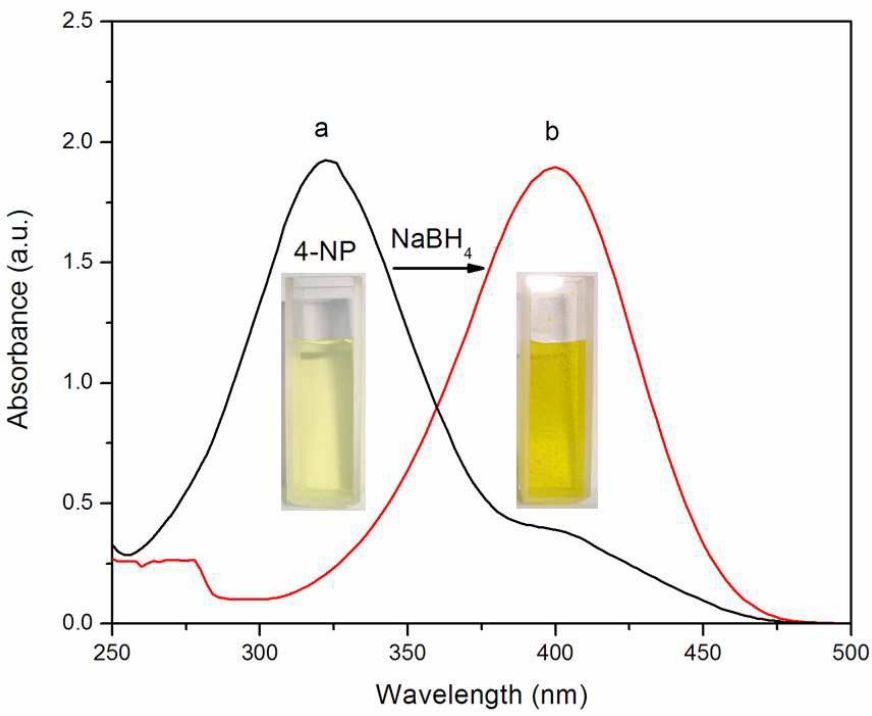

Fig. 6

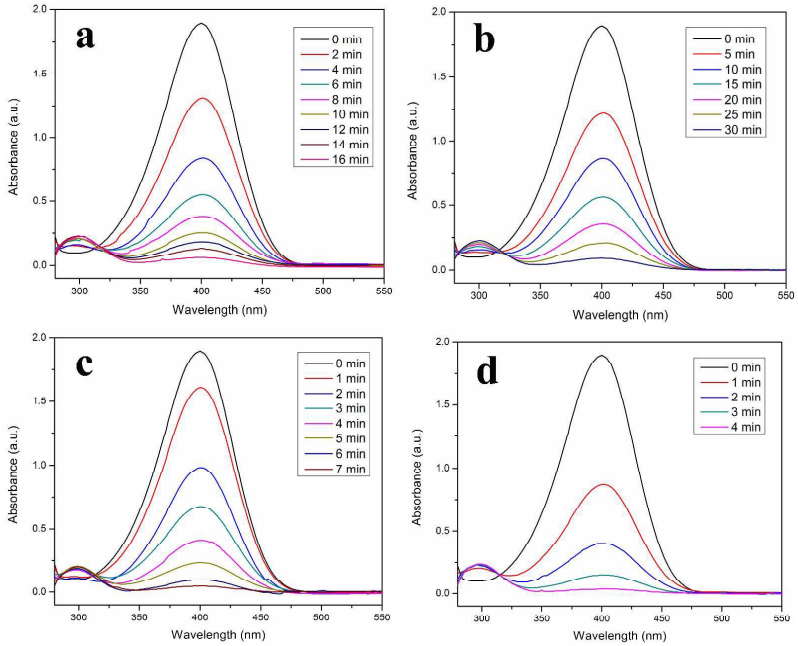

Fig. 7

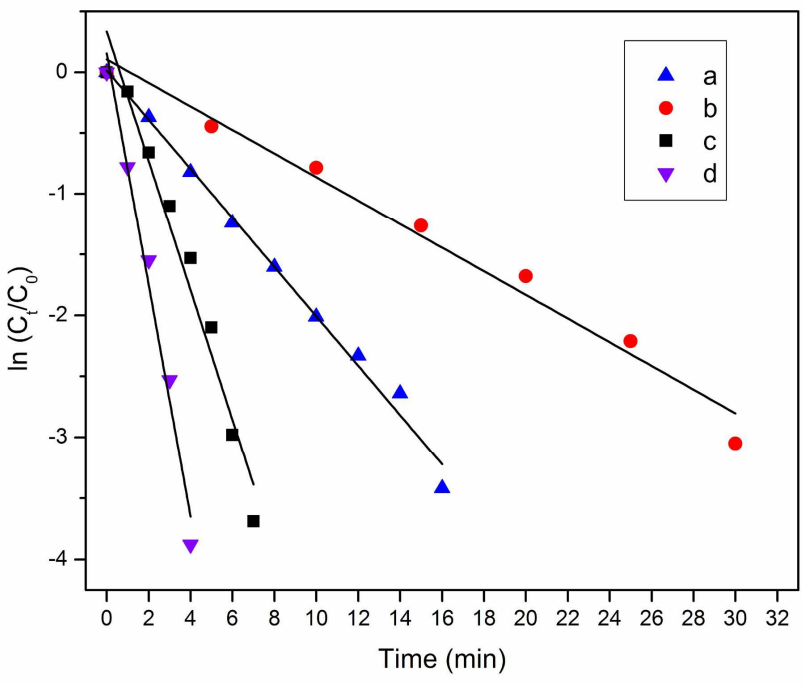

Fig. 8

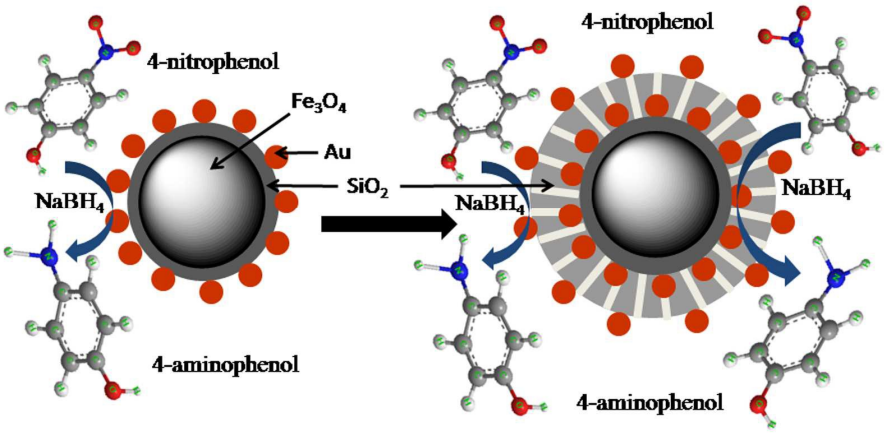

Fig. 9

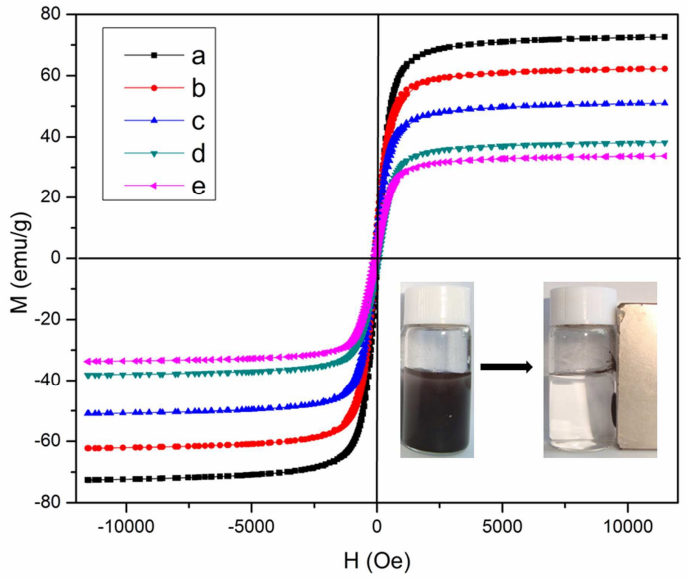

Fig. 10

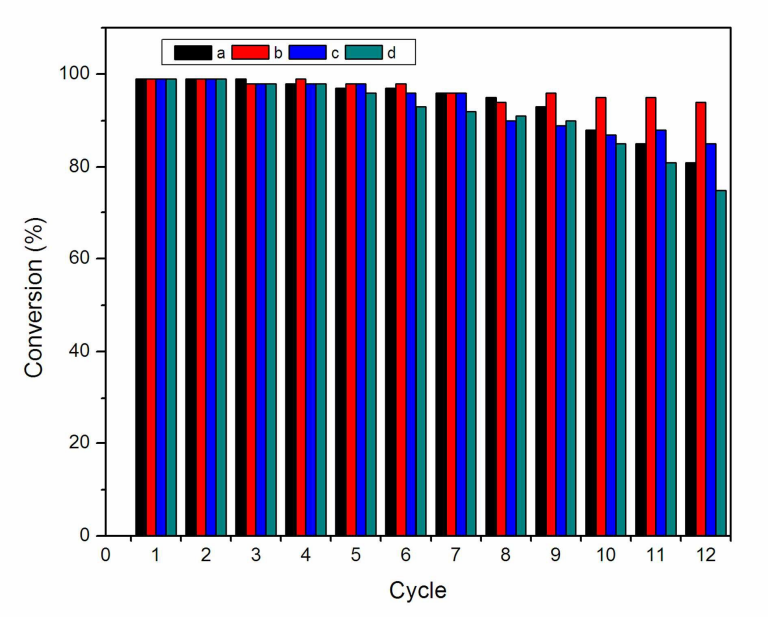

Fig. 11

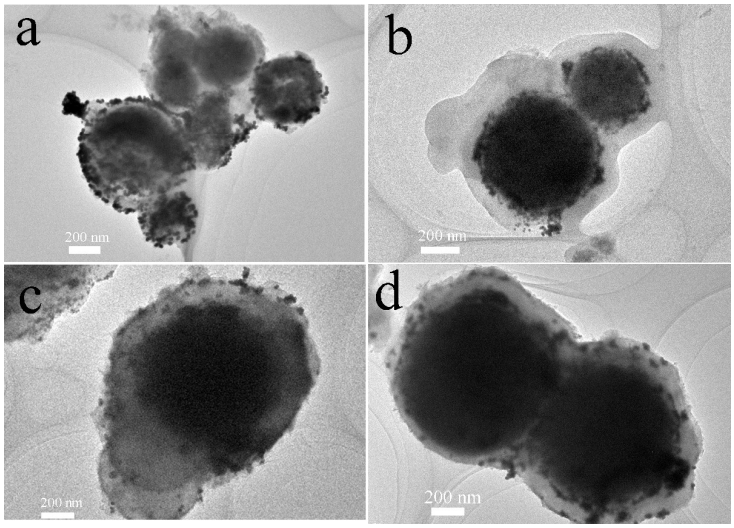

Fig. 12

Nanocomposite catalysts, with single and double gold layers, and with one gold layer and one silver layer were prepared through simple steps, and showed excellent activity in reduction of nitrophenols.